HHS Public Access

Author manuscript

*Stem Cell Rev*. Author manuscript; available in PMC 2015 June 02.

Published in final edited form as:

*Stem Cell Rev*. 2015 June ; 11(3): 511–525. doi:10.1007/s12015-014-9549-5.

# Human vascular tissue models formed from human induced pluripotent stem cell derived endothelial cells

**David G. Belair**[1], **Jordan A. Whisler**[2], **Jorge Valdez**[3], **Jeremy Velazquez**[3], **James A. Molenda**[1], **Vernella Vickerman**[4], **Rachel Lewis**[5], **Christine Daigh**[5], **Tyler D. Hansen**[1], **David A. Mann**[5], **James A. Thomson**[4,6,7], **Linda G. Griffith**[3], **Roger D. Kamm**[2,3], **Michael P. Schwartz**[1], and **William L. Murphy**[1,8,9,*]

[1]Department of Biomedical Engineering, University of Wisconsin-Madison, Madison, WI USA

[2]Department of Mechanical Engineering, Massachusetts Institute of Technology, Cambridge, MA USA

[3]Department of Biological Engineering, Massachusetts Institute of Technology, Cambridge, MA USA

[4]Morgridge Institute for Research, Madison, WI USA

[5]Cellular Dynamics International, Inc., Madison, WI USA

[6]Department of Cell and Regenerative Biology, University of Wisconsin-Madison, Madison, WI USA

[7]Department of Molecular Cellular and Developmental Biology, University of California-Santa Barbara, Santa Barbara, CA

[8]Material Science Program, University of Wisconsin-Madison, Madison, WI USA

[9]Department of Orthopedics and Rehabilitation, University of Wisconsin-Madison, Madison, WI USA

## Abstract

Here we describe a strategy to model blood vessel development using a well-defined iPSC-derived endothelial cell type (iPSC-EC) cultured within engineered platforms that mimic the 3D microenvironment. The iPSC-ECs used here were first characterized by expression of endothelial markers and functional properties that included VEGF responsiveness, TNF-α-induced upregulation of cell adhesion molecules (MCAM/CD146; ICAM1/CD54), thrombin-dependent barrier function, shear stress-induced alignment, and 2D and 3D capillary-like network formation in Matrigel. The iPSC-ECs also formed 3D vascular networks in a variety of engineering contexts, yielded perfusable, interconnected lumen when co-cultured with primary human fibroblasts, and aligned with flow in microfluidics devices. iPSC-EC function during tubule network formation, barrier formation, and sprouting was consistent with that of primary ECs, and the results suggest a

[*]**Corresponding author**, William L. Murphy, can be contacted at Wisconsin Institute for Medical Research II, 1111 Highland Avenue Room 5405, Madison, WI 53705. Phone: (608)262-2224. Email correspondence: wlmurphy@wisc.edu (W.L. Murphy).

**Conflict of Interest Disclosure:** J.A.T. is a founder, stockowner, consultant, and board member of Cellular Dynamics International, Inc. D.A.M., R.L. and C.D. are employed by, and have a financial interest in, Cellular Dynamics International Inc.

VEGF-independent mechanism for sprouting, which is relevant to therapeutic anti-angiogenesis strategies. Our combined results demonstrate the feasibility of using a well-defined, stable source of iPSC-ECs to model blood vessel formation within a variety of contexts using standard *in vitro* formats.

**Keywords**

Stem Cell; Induced Pluripotent Stem Cell; Endothelial Cell; Angiogenesis; Vascular Model; Vascular Function; Tubulogenesis; Migration; Sprouting; Barrier Function

## INTRODUCTION

The lack of a functional vasculature in healing or transplanted tissues has motivated efforts to deconstruct the critical factors that stimulate blood vessel maintenance and growth[1, 2]. Hydrogels with defined extracellular matrix (ECM) properties[3–5] and microfluidics approaches for controlling soluble gradients, flow, and surface shear[6, 7] have been used to model vasculature in 3-dimensional (3D) microenvironments[8–10]. However, the complexity of blood vessel specification and heterogeneity of primary human endothelial cells[11] limits the robustness of engineered vascular models. Robust models of vasculature are likely required for emerging tissue modeling applications that rely on standardization and quantitative readouts to enable toxicity and drug screening[12–15].

Human pluripotent stem cells have received increasing attention for tissue modeling applications, as they provide a well-defined source of tissue-specific cell types[16–18]. Induced pluripotent stem cells (iPSC) are a particularly promising cell source for modeling tissue development and pathologies associated with specific genetic defects, since patient-derived tissues can be generated using both disease-relevant cell lines and control cell lines[19–22]. Multiple strategies for human endothelial cell (EC) differentiation have been reported for both embryonic stem cells and induced pluripotent stem cells[23–28]. Thus, human iPSC-derived endothelial cells (iPSC-ECs) represent a potentially valuable tool for the development of robust and reproducible vascular tissues for disease modeling and screening applications[12–15].

Here we demonstrate that human iPSC-ECs reproduce functional properties reported for primary ECs using multiple engineered *in vitro* environments. The iPSC-ECs were characterized by expression of characteristic EC markers, including >90% PECAM1$^+$/ENG$^+$ (CD31$^+$/CD105$^+$), observed across 3 separate production lots and 6 passages in culture. The iPSC-ECs were characterized by VEGF responsiveness in multiple contexts, thrombin-dependent barrier function, acetylated LDL uptake, and unregulated expression of characteristic blood vessel cell adhesion molecules MCAM (CD146) and ICAM-1 (CD54) in response to TNF-α. Further, iPSC-ECs assembled into capillary-like networks on 2D substrates and within 3D Matrigel culture, aligned with the direction of fluid flow, and formed perfusable lumen within microfluidics devices. A quantitative sprouting assay with iPSC-ECs was developed and demonstrated dependence on vascular endothelial growth factor (VEGF) and fibroblast growth factor-2 (FGF-2) signaling, as well as microtubule stability, in agreement with previous studies. The sprouting assay identified context-specific

pharmacological inhibition with implications for screening and development of anti-angiogenic drugs. Finally, results showed that synergistic signaling through FGF-2 and VEGF enhanced iPSC-EC sprouting, although VEGF/VEGF receptor 2 (VEGFR2) signaling was not necessary to induce sprout formation. Taken together, our results demonstrate the suitability of a defined human iPSC-EC line for investigating vascular biology in multiple distinct experimental contexts.

## RESULTS

### iPSC-ECs robustly express endothelial markers and respond to VEGF signaling

iPSC-ECs exhibited function and marker expression consistent with previous studies of primary endothelial cells. iPSC-ECs actively internalized acetylated LDL as a substrate (Suppl. Fig. 1A)[29], stained positive for UEA-1 (Fig. 3D)[30], and expressed von Willebrand factor (vWF, Suppl. Fig. 1C–D), CD31 (PECAM1, Fig. 1A–C), endoglin (ENG/CD105; Fig. 1A, 1C), VE-cadherin (CD144, Fig. 1B), and VEGFR2/KDR (Fig. 1D) with high purity[25]. Further, iPSC-ECs proliferated in response to VEGF-A (hereafter referred to as VEGF) in a dose-dependent fashion (Fig. 1E). The proliferative response for iPSC-ECs was reduced by the VEGFR2 inhibitor SU1498 [31] (Fig. 1F), which is consistent with a role of VEGF/VEGFR2 signaling for promoting normal endothelial cell function[32, 33]. Greater than 90% of the iPSC-EC population was $CD31^{+}/CD105^{+}$ from three independent production runs and over six passages in culture (Fig. 1C). Thus, the iPSC-ECs stably expressed purity markers during routine culture and exhibiting functional characteristics consistent with primary ECs.

### iPSC-ECs exhibit barrier function, exhibit wound healing behavior, and respond to inflammatory stimuli

Endothelial cells change their barrier properties during wound healing and inflammation[34] and differentially express the adhesion molecules intercellular adhesion molecule (ICAM) and melanoma cell adhesion molecule (MCAM) to recruit circulating immune and progenitor cells[35]. We thus characterized iPSC-EC barrier function in response to a wound healing stimulus and marker expression upon cytokine challenge. ZO-1 expression at the cell borders for iPSC-ECs (Fig. 2A) provided evidence of tight junction formation[36, 37]. We further investigated the ability of iPSC-ECs to form a barrier using an impedance-based platform to assess barrier function (see Methods)[34]. Impedance measurements demonstrated that iPSC-ECs formed functional barriers that were disrupted by thrombin treatment (Fig. 2B) and were recoverable at lower continuous thrombin doses (Fig. 2B; Blue and Green traces). Thus, iPSC-ECs exhibited reversible changes in barrier function consistent with previous studies of EC monolayers treated with edemagenic agents (including thrombin) at low concentrations[38, 39]. We further investigated the capacity for iPSC-ECs to express cell adhesion molecules (CAMs) in response to TNF-α stimulation (Fig. 2C–F), thus recapitulating EC properties necessary for cell recruitment during wound healing and inflammation[35]. Flow cytometry analysis demonstrated that TNF-α treatment induced upregulation of ICAM-1 (CD54; Fig. 2C–D) and MCAM (CD146; Fig. 2E–F), which are expressed by ECs to promote attachment of immune and progenitor cells to blood vessels[35]. These results indicate that iPSC-ECs functionally respond to stimuli required

for wound healing, and suggest that iPSC-ECs are a well-defined cell source for investigating blood vessel properties *in vitro* and understanding the transport of solutes or cells across blood vessel barriers[40].

## iPSC-ECs align in response to shear stress and form capillary-like networks with perfusable lumen

A hallmark for endothelial cell function is the capacity to form capillary-like networks in 2D and 3D contexts[3–5, 23, 41–46]. Here, iPSC-ECs organized into cord-like networks on Matrigel-coated tissue culture polystyrene (TCP; Fig. 3A) or on thick Matrigel slabs (Fig. 3C)[43, 44], with similar results observed for HUVECs (Fig. 3B; Matrigel-coated TCP). iPSC-ECs also formed 3D capillary-like networks when encapsulated in Matrigel (Fig. 3F). iPSC-ECs (Fig. 4D,F) and HUVECs (Fig. 4E) appeared to elongate towards the central axis of flow, but iPSC-ECs remained rounded (Fig. 4C) during static culture in a perfusable bioreactor[47], consistent with a possible role for shear stress in directing cytoskeletal organization[48]. To confirm the capacity for iPSC-ECs to align in response to shear stress, we used monolayer culture within a microfluidics device to quantitatively control chamber geometry and flow rate (Fig. 3E). An applied shear stress of 20 dyne/cm$^2$ induced iPSC-ECs to elongate in the direction of 2D flow after 72hr (Fig. 4A,B), which is consistent with the behavior of primary endothelial cells as previously measured[48]. Finally, iPSC-ECs seeded in fibrin gels within a microfluidics device and co-cultured with normal human lung fibroblasts assembled into three dimensional, inter-connected capillary networks and formed cord-like structures containing visibly hollow lumens (Fig. 5A). The presence of interconnected vascular lumen for iPSC-ECs in fibrin gels was confirmed using epifluorescence microscopy to document the transport of 4 μm diameter beads through the capillary network (Fig. 5B, Suppl. Movie 1).

## VEGF/VEGFR2 signaling influences iPSC-EC sprouting

Endothelial cell sprouting comprises the initial stage of angiogenesis, and assays for EC sprouting[49–52] represent valuable tools for the screening and development of angiogenesis regulators[53]. We developed and characterized an *in vitro* sprouting assay (Fig. 6A) to examine iPSC-EC behavior in response to stimulation by VEGF or inhibition by a library of pharmacological inhibitors (Fig. 6B). iPSC-ECs exhibited sprouting (Fig. 7C), migration (Fig. 8C), and invasion (Suppl. Fig 2C) that was dependent on the concentration of a microtubule polymerization inhibitor (nocodazole), which is consistent with a role of microtubules for regulating endothelial cell function in different contexts[54]. Importantly, sprouting behavior was dependent on the concentration of VEGF (Fig. 7A), consistent with VEGF-dependent sprouting of primary endothelial cells[50, 55]. Inhibition studies in VEGF-containing medium demonstrated that sprouting was abolished in the presence of a VEGFR2 inhibitor (SU1498), a tyrosine kinase inhibitor (Sunitinib) (Fig. 6E), and a FGFR/VEGFR2 inhibitor (SU5402) (Fig. 7B), confirming that VEGF/VEGFR2 signaling can induce EC sprouting. We further examined the effect of pharmacological inhibitors on iPSC-EC sprouting behavior in culture with either Growth Medium containing multiple growth factors including VEGF and FGF-2, or Starvation Medium containing VEGF alone (Fig. 6B). Results demonstrated that sprouting in Starvation Medium with VEGF alone was inhibited in the presence of anti-angiogenic agents: receptor tyrosine kinase inhibitors

(SU1498, Sunitinib), a MEK inhibitor (PD0325901), a non-specific protein kinase inhibitor (Staurosporine), and a histone deacetylase inhibitor (Trichostatin-A) (Fig. 6B). Interestingly, sprouting behavior in the presence of Growth Medium was unaffected by treatment with SU1498 (Fig. 6B), a VEGFR2 inhibitor, and the longest continuous skeleton (defined as the longest branched skeleton for each condition) was significantly higher with SU1498 treatment versus the VEGF-only condition without inhibition (Fig. 6D). These results suggest that VEGF/VEGFR2 signaling can induce iPSC-EC sprouting, and the influence of VEGF/VEGFR2 is dependent on the characteristics of the cell culture medium.

We hypothesized that the mechanism for VEGF-induced sprouting involved increased migration of iPSC-ECs, which is consistent with the role of VEGF for inducing endothelial cell chemotaxis[56, 57]. VEGF promoted iPSC-EC migration in a dose-dependent fashion (Fig. 8D), and treatment with a specific VEGFR2 inhibitor, SU1498, abolished iPSC-EC migration (Fig. 8E), suggesting that VEGF induced iPSC-EC migration through VEGFR2. Treatment with a FGFR/VEGFR2 inhibitor (SU5402) inhibited iPSC-EC migration (Fig. 8B) and invasion (Suppl. Fig. 2B), further demonstrating that single-cell migration and invasion of iPSC-ECs was dependent on VEGF/VEGFR2 signaling. Taken together, our results suggest that VEGF/VEGFR2 was sufficient but not necessary to promote iPSC-EC sprouting, and VEGF/VEGFR2 signaling can promote single-cell migration whereas FGF2/FGFR signaling may promote sprouting independently of VEGF.

## Discussion

Current *in vitro* models of blood vessel function typically use primary human ECs that are derived from patients and expanded *in vitro*[58]. However, primary ECs exhibit tissue-specific heterogeneity[11, 59] and present challenges for robust design of *in vitro* angiogenesis assays, including drug screening assays. Human pluripotent stem cells provide unique advantages for deriving tissue-specific cell types, and numerous protocols exist to differentiate stem cells into ECs[23–28]. iPSCs are a promising source of stem cells that can be readily differentiated to ECs and exhibit a diversity of vascular functions[60]. Here we used iPSCs-ECs, which exhibited a phenotype consistent with primary ECs (Figs. 1–2; Suppl. Fig. 1), exhibited thrombin-dependent barrier function (Fig. 2B), and responded to inflammatory stimulus (Fig. 2 C–F). Thus, iPSC-ECs provide a robust model system that is consistent with the phenotype and barrier function of primary ECs.

Angiogenesis is a complex process that involves a cascade of signaling molecules and regulatory events[61]. Here we found that iPSC-ECs responded to pro-angiogenic growth factors (*e.g.* VEGF; Fig. 1E–F, 7A, 8D), assembled into tubule networks in 2D (Fig. 3A–D) and 3D matrices (Fig. 3F), and formed perfusable tubule networks in 3D culture (Fig. 5, Suppl. Movie 1). iPSC-ECs aligned with flow in 2D (Fig. 4A–B) and elongated towards the axis of flow in 3D (Fig. 4C–F), consistent with a role of shear stress in inducing EC cytoskeletal arrangement[48]. The stem cell derived ECs exhibited sprouting in 3D spheroid culture that was dependent on VEGF concentration (Fig. 7A) and FGFR/VEGFR2 signaling (Fig. 6B, 7B), consistent with the role of VEGF/VEGFR2 and FGF2/FGFR signaling for promoting endothelial cell sprouting[62]. We also observed complete inhibition of iPSC-EC sprouting in the presence of PD0325901 (Fig. 6B), a MAPK/ERK inhibitor, which is

consistent with the role of ERK1/2 to promote sprouting angiogenesis[63]. Together these results demonstrate that iPSC-ECs exhibit functional properties consistent with those reported for primary ECs and associated with those needed for robust screening assays.

We further investigated the utility of iPSC-ECs as a well-defined cell type to screen for the influence of pharmacological agents using a quantitative angiogenesis assay. Known pharmacological protein kinase inhibitors that have been previously investigated as therapeutic antiangiogenic agents disrupted iPSC-EC sprouting in our experiments, including inhibitors of MEK (PD0325901 [63]), protein kinases (Staurosporine[64]), histone deacetylases (Trichostatin A[65]), and receptor tyrosine kinases (Sunitinib[66]). SU1498 (tyrphostin)[31] and Sunitinib blocked sprouting for iPSC-ECs in serum-containing medium with only VEGF (Fig. 6E), which confirms a role of VEGF/VEGFR2 for inducing sprouting[50, 67]. Interestingly, VEGFR2 inhibition with SU1498 did not affect iPSC-EC sprouting in Growth Medium containing multiple growth factors including VEGF and FGF-2 (Fig. 6B), and the longest continuous skeleton was increased relative to VEGF-containing Starvation Medium (Fig. 6D), suggesting EC sprout length was enhanced by VEGFR2 inhibition. However, iPSC-EC sprouting was completely abolished by the combined VEGFR2/FGFR inhibitor SU5402 [68] (Fig. 6B) suggesting a role for FGF2/FGFR signaling in promoting maximal sprout formation that is consistent with previous studies examining bovine luteal endothelial cell tube formation[62]. These results are also consistent with previously reported roles for FGF2/FGFR signaling in promoting EC sprouting[50, 62, 69] and increasing vascular integrity independently of VEGF/VEGFR2 signaling[70]. We posit that VEGF signaling may provide a “switch” from a sprouting phenotype to a single cell migration phenotype that is relevant to therapeutic strategies and may provide an explanation for the limited efficacy of anti-angiogenesis therapies targeting VEGF alone. Our results suggest that FGF2/FGFR signaling may be a useful target for increasing the efficacy of anti-angiogenic therapies that are currently based on VEGF/VEGFR2 inhibition.

Our results also provide evidence that enhancement of sprouting angiogenesis by VEGFR2 inhibition is due to a role for VEGF signaling in modulating EC phenotype (Fig. 6D–E, Fig. 7A–B). While cumulative sprouting length was unaffected by VEGFR2 inhibition in Growth Medium, sprouting was abolished by VEGFR2 inhibition in VEGF-containing medium as well as by combined FGFR/VEGFR2 inhibition in both Growth and VEGF-containing medium (Fig. 6B). However, VEGF/VEGFR2 inhibition by SU1498 in Growth Medium increased the longest continuous skeleton relative to VEGF-containing Starvation Medium (Fig. 6D). Since the “cumulative sprout length” measurement here represents both single-cell migration and sprouting, our data suggest that a larger value of the “longest continuous skeleton” corresponded to increased sprouting and decreased single-cell migration in Growth Medium containing SU1498. This conclusion is supported by evidence showing that VEGFR2 inhibition abolished VEGF-mediated single-cell migration (Fig. 8E). Angiogenesis requires a complex interplay of numerous growth factors that are tightly regulated[61]. Thus, it is reasonable to expect that synergy between multiple pro-angiogenic growth factors can modulate the process of sprouting angiogenesis, and VEGF inhibition may enhance sprouting angiogenesis by amplifying the effects of other pro-angiogenic growth factors, including FGF2 [61]. Based on the combined results, we hypothesize that

VEGF inhibition decreases EC single cell migration and may promote sprouting, which could have important implications related to the confounding results of anti-VEGF therapy to reduce tumor growth[71].

Our assessment of sprouting behavior in iPSC-ECs showed inhibition with specific anti-angiogenic agents, and the inhibition was dependent on the characteristics of the cell culture medium. SU5402 and nocodazole exhibited $IC_{50}$ values of 4 and 8nM respectively for inhibiting iPSC-EC proliferation (Suppl. Fig. 3B–C), and exhibited $IC_{50}$ values of 730nM and 100nM respectively for inhibiting iPSC-EC sprouting (Fig. 7 B,C). These results illustrate that nocodazole and SU5402 potencies were 13-fold and 200-fold higher, respectively, for inhibiting proliferation versus inhibiting sprouting. Proliferation and sprouting inhibition with nocodazole agrees with the previously measured potency of nocodazole for inhibiting cell proliferation and tubule network formation[54]. Further, SU5402 inhibition of iPSC-EC proliferation is in agreement with previously measured potency of SU5402 for inhibiting primary EC proliferation[68]. The observed inhibition of VEGF-dependent iPSC-EC sprouting at 1 μM SU5402 is consistent with previously measured SU5402 inhibition of VEGF- and FGF2-dependent tubule network formation for primary ECs[62, 72]. These studies highlight the importance of context for drug screening applications, as growth factor signaling[61, 73, 74] and the cellular cytoskeleton[54] exhibit different effects on EC function (*i.e.* proliferation, migration, tubule network formation, and sprouting) during angiogenesis.

## Conclusions

Stem cell technology enables the development of tissue models that use differentiated iPSCs to provide standardized quantitative readouts for tissue engineering, drug development, toxicity screening, and disease modeling. Here we demonstrate the utility of a defined iPSC-EC source for modeling vascular tissue formation within 3D microenvironments, and for profiling the influences of specific pharmacologic agents. Our results demonstrate the potential for a well-defined source of iPSC-ECs to investigate vascular biology within engineering contexts, including single cell and spheroid encapsulation within natural matrices and culture within microfluidics devices and bioreactor systems. The iPSC-ECs expressed EC markers consistent with primary ECs and exhibited functional EC properties, such as the uptake of LDL, formation of a thrombin-dependent barrier, cytoskeletal rearrangement in the presence of flow, and perfusable tubule network formation in 3D contexts. Further, iPSC-ECs responded to wound healing stimuli by upregulating expressing of ICAM and MCAM, and exhibited VEGF-dependent proliferation and sprouting. We developed a novel sprouting assay with iPSC-ECs that quantitatively assessed growth factor stimulation and pharmacological inhibition. The sprouting model provided new insight into synergistic roles for VEGF and FGF signaling during angiogenesis wherein inhibition of VEGFR2 signaling enhances maximal sprout formation. Thus, our results demonstrated that VEGF/VEGFR2 signaling is a sufficient but not necessary condition to induce iPSC-EC sprouting. Hence, iPSC-ECs provide a robust, stable, and reproducible model system for *in vitro* angiogenesis that enables basic biological research and molecular pharmacology studies with the potential to generate donor specific disease models.

## MATERIALS AND METHODS

### Cell culture

iPSC-ECs used for all experiments were obtained from Cellular Dynamics International, Inc. (CDI, Madison, WI) and cultured according to the manufacturer's protocols. Briefly, iPSC-ECs were plated onto Fibronectin (3 μg/cm$^2$, Invitrogen) coated tissue culture plates at 10,000–15,000 cells/cm$^2$ and passaged every three to four days with TrypLE (Invitrogen). iPSC-ECs were cultured using VascuLife VEGF Medium (Lifeline Cell Technologies, Frederick, MD) supplemented with the complete growth factors per the kits. Here, only 10 mL of the glutamine solution was added per 500 mL media and 50 mL of the CDI provided supplement replaced the VascuLife FBS component. Hereafter, this medium is referred to as "Growth Medium", and cells in all contexts were cultured at 37°C, 5% $CO_2$, 5% $O_2$

### Flow cytometry

iPSC-ECs were harvested with TrypLE and stained with either isotype control or antigen-specific antibodies. Cell-surface antigen expression was analyzed using fluorescently conjugated antigen-specific antibodies against VEGFR2/KDR (R&D Systems, clone 89106), CD31 (BD Biosciences, clone WM59), CD105 (eBiosciences, clone SN6) and CD144 (eBiosciences, clone 16B1). The cells were also tested for contaminating iPSCs using an antibody against TRA-1-81 to confirm a negative result (Stemgent, San Diego, CA). Internal antigen expression was analyzed using methanol fixed cells permeabilized with PBS + 0.1% saponin/BSA. Unconjugated polyclonal rabbit anti-human von Willebrand Factor (Dako, Carpinteria, CA) was detected with an Alexa Fluor 488 goat anti-rabbit secondary antibody (Molecular Probes, Eugene, OR). Cells were analyzed on an Accuri flow cytometer (BD Biosciences) using propidium iodide, when appropriate, to exclude dead cells. iPSC-ECs exhibited a purity of ≥ 90% as measured by high coexpression of CD31 with CD105 or CD144 by flow cytometry.

### Tube formation on Matrigel

Matrigel (0.2 mL; BD Biosciences) was added to each well of a 24-well tissue-culture plate and allowed to solidify at 37°C for at least 30 minutes. Following gelation, 0.2 mL of a cell suspension containing $1 \times 10^5$ iPSC ECs in Growth Medium was placed on top of the Matrigel. The cultures were incubated at 37°C, 5% $CO_2$, and observed at 24, 48, and 72 hours for observation of cellular formation into capillary-like structures. ***Ulex staining:*** Matrigel tubes were stained with the lectin Ulex europaeus (Sigma) after 24 hours to confirm the presence of human endothelial cells in the vessel-like formations. Briefly, Growth Medium was removed from the Matrigel layer and tubes were incubated with 10 μg/ml Ulex for 30 minutes at room temperature followed by imaging.

### Immunostaining

Cells were stained as below, washed, and nuclei were counterstained using Hoechst 33342 (Invitrogen) for imaging. ***AcLDL:*** Analysis for the acetylated LDL receptor mediated uptake of AcLDL was performed overnight at 37°C, 5% $CO_2$ in iPSC EC growth medium containing 2.5 μg/ml Alexa Fluor 594 AcLDL (Molecular Probes) followed by imaging.

Prior to immunostaining, proprietary CDI supplement contained in the medium was reduced to ≤5%. ***vWF:*** iPSC-ECs were fixed with methanol, blocked for 30 min. with PBS containing 10% FBS + 0.1% $NaN_3$, and stained with 0.5 μg/ml vWF for 1 hour. Secondary antibody was added at a 1:500 dilution for 30 min. Antibodies were diluted in PBS containing 2% FBS + 0.1% $NaN_3$ and were the same as those used in flow cytometry for the detection of the von Willebrand factor/factor VIII complex (Dako, Carpinteria, CA). All staining was carried out at room temperature. ***Z0-1:*** The tight junction protein ZO-1 analysis on the iPSC-ECs was carried out using an Alexa Fluor 488 ZO-1 antibody (Molecular Probes). Cells were fixed with 4% paraformaldehyde, permeabilized with PBS + 0.1% saponin/BSA, and stained overnight with 2 μg/ml Z0-1 at 4°C prior to imaging.

## Barrier Function

To measure barrier function and endothelium permeability of iPSC-ECs, an impedance-based platform was employed (xCelligence, ACEA system). In brief, one E-plate Cardio 96 plate was pre-coated with fibronectin (15 μg/$cm^2$, Invitrogen) for 1 hour at room temperature. Fibronectin solution was then aspirated from wells and replaced with 0.15 mL per well of Growth Medium. The plate was incubated for 5 minutes, after which a background measurement was recorded. Wells were aspirated, and iPSC-ECs were seeded in Growth Medium at 64,000 cells/mL in a final volume of 0.15 mL/well (~30,000 cells/$cm^2$). Cells were incubated for 30 minutes at room temperature and transferred to 37°C, 5% $CO_2$ for 2 days. At day 2 post-plating, 0.1 mL of spent medium was exchanged with 0.13 mL of fresh 37°C Growth Medium (leaving a total of 0.18 mL in each well), and plate was incubated for at least 1 hour at to 37°C, 5% $CO_2$. A background measurement was recorded before the start of the experiment. Barrier function was disrupted by the addition of 20 μL of a 10× solution of thrombin (Sigma) to each well to achieve a final concentration of 0 (control), 0.5, 1, 1.5, or 5 U/ml. The cellular response to thrombin was then monitored for 2.5 hours to observe recovery of the barrier function.

## Proliferation Assay

The proliferation of iPSC-ECs was assessed using the Cell Titer-Glo Luminescent Cell Viability Assay (Promega). Cells were plated to a 96-well tissue culture plate (Corning) pre-coated with fibronectin (3 μg/$cm^2$, Invitrogen) at 5,000 cells/$cm^2$ in a final volume of 100 μL/well. The plate was incubated at 37°C, 5% $CO_2$, 5% $O_2$ for 24 hours at which time the medium was exchanged with 100 μL/well of fresh Growth Medium or Starvation Medium, containing VascuLife Basal Medium with 4 mM L-glutamine and 0.1 vol.% iPSC-EC supplement (CDI). Cells in Growth Medium were assayed at 72, 96, and 120 hours (days 3, 4, and 5) post-plating, with an additional fresh medium exchange at 96 hours post-plating. At 48 hours post-plating, cells in Starvation Medium were fed fresh Starvation Medium containing a seven-point titration (2-fold dilution series) of VEGF with a maximal highest concentration of 80 ng/ml). In addition, a dilution series of the VEGFR2-inhibitor (Tyrphostin SU1498; Sigma) was also prepared with the highest concentration of 40 μM in the presence or absence of 5 ng/ml of VEGF. 48 hours after treatment, the cells were fed with fresh Starvation Medium containing the same compound titrations and assayed the following day (totaling day 5 post-plating). The amount of cellular ATP was quantified using Cell Titer-Glo per the manufacturer's instructions. Luminescence readings were taken

using the Tecan GENios Pro Microplate Reader (1 second integration time/sample). Proliferation fold induction was calculated relative to the values obtained with cells maintained in starvation medium. Standard deviation was calculated from triplicate wells.

### 2D Shear Stress Experiments

To investigate the response to shear stress, endothelial monolayers were cultured under static and flow conditions. For dynamic cultures, monolayers were subjected to unidirectional flow at 20 dyne/cm$^2$ for 72 hours using a software controlled perfusion system (Ibidi pump system, red perfusion set: 15cm ID 1.6mm, Ibidi) according to the manufacturer guidelines. Confluent endothelial monolayers were generated by seeding single cells on fibronectin coated slides (μ-slide I$^{0.6}$, IbiTreat) at $1\times10^5$ cells/cm$^2$ and subsequently cultured under static conditions overnight in growth medium at 37°C and 5% $CO_2$. Prior to flow initiation, culture medium was exchanged for fresh growth medium supplemented with 10% FBS. At the end of the experiment, monolayers were fixed (4% paraformaldehyde) and stained for cell-cell junctions and nuclei with anti-VE-Cadherin and DAPI respectively.

### Microfluidic Experiments

The procedure for forming perfusable microvascular networks in a multi-culture microfluidic system is described in detail elsewhere[75]. Briefly, a PDMS device containing three parallel gel regions – each separated by a medium channel – was permanently bonded to a glass coverslip. The middle gel region was filled with a 2.5 mg/ml fibrin gel containing iPSC-ECs at 3.5 million cells/ml. The two side gel regions were filled with fibrin gel containing normal human lung fibroblasts (NHLFs; Lonza, MD, USA) with the same gel concentration and cell density as for iPSC-ECs. The devices were incubated at room temperature for 10 min to allow the gel to polymerize before adding warm growth medium supplemented with 250 nM sphingosene-1-phosphate (S1P; Sigma, MO, USA) to the medium channels. Fresh medium was replenished every two days. After 4 days, the devices were fixed with 4% paraformaldehyde and stained for actin and nuclei with phalloidin and DAPI respectively. To demonstrate flow through the live and fixed networks, we perfused the system with medium containing 4 μm fluorescent microspheres (Life Technologies; NY, USA) by imposing a hydrostatic pressure drop across the vascularized gel region. This was readily accomplished by filling the medium channel on one side of the vascularized gel region 1–2 mm higher than the other side.

### Alignment and Network Formation Assay

iPSC-ECs (passage 3) were harvested with TrypLE and resuspended in 4°C Matrigel (BD Biosciences) at 5 million cells/ml. 200 μL of cell-containing Matrigel solution were placed onto circular uncoated 1 cm diameter scaffolds (Zyoxel, LC15) held down by retaining rings against LiverChip™ filters (Zyoxel, LC17) within a LiverChip™ perfusion plate (Zyoxel, LC-CP and LC-PP) and allowed to form hydrogels (8 hydrogels of 200 μL volume each) at room temperature for 10 minutes before adding 1.7 mL of medium, which was replenished every other day. The perfusion plate was assembled and operated as illustrated in Fig. 3E according to the manufacturer guidelines. The medium flow was set to 0.3 μL/s downward into the hydrogel throughout the entire timespan of the experiment. At the indicated times,

two scaffolds were sacrificially removed from the perfusion plate and incubated in media in the presence of 1 μg/mL calcein AM (Life Technologies) for 40 minutes at 37°C and imaged immediately after using an inverted epifluorescence microscope.

## Sprouting Assay

Sprouting behavior of iPSC-ECs was assessed by culturing the cells in a spheroid as shown (Fig. 6A). iPSC-ECs at between Passage 2–6 were seeded into non-adherent round bottom 96 well plates (Corning) at 500 cells/well in 20 vol.% methylcellulose (Sigma; 600 mg/L in phosphate buffered saline) and 80 vol.% Starvation Medium (with 10 vol.% CDI supplement). After 24 hours, half of the medium was replaced with 40 vol.% Matrigel in PBS, making a gel containing 20 vol.% Matrigel after 4 hours at 37°C, 5% $CO_2$, and 95% relative humidity. Subsequently, the culture conditions described in Figs. 6–7 were added at 100 μL per well. For inhibition studies, either Starvation Medium with 20 ng/mL VEGF or Growth Medium was added containing 0.1 vol.% of inhibitor stock solutions. For VEGF titration, a 2-fold serial dilution was prepared in Starvation Medium. Finally, for nocodazole and SU5402 titration, a 2-fold serial dilution was prepared in Starvation Medium with 20 ng/L VEGF. Cultures were maintained for 6 days, with medium changes every other day. On the final day, cells were stained with 2 μg/mL Calcein-AM and 4 μg/mL Ethidium Homodimer-1, and cells were imaged using epifluoresence. Images were processed using ImageJ. Specifically, images were uniformly thresholded and auto-contrasted using the Otsu method, and the Skeleton plugin was utilized to skeletonize fluorescent images and analyze the total length of the skeletonized network (in pixels). For the analysis in Fig. 6D, the "longest continuous skeleton" measurement was defined as the skeleton with the largest cumulative length of branches in a given skeleton identified via the skeleton analysis. Conditions were performed in sextuplicate and compared via two-tailed Student's t-test at p-value<0.05. For statistical analysis of growth factor and inhibitor concentration screening, sigmoidal regression analysis was performed in Prism (GraphPad), and $IC_{50}$ values and $EC_{50}$ values were calculated for each condition. Data is presented as the mean value +/− one standard deviation.

## Migration Assay

To measure migration of iPSC-ECs, an impedance based system was employed (xCelligence, ACEA system). In brief, the underside of the upper chamber of CIM-plates was pre-coated with fibronectin (15 $\mu g/cm^2$, Invitrogen) for 1 hour at room temperature. Medium conditions were prepared in Starvation Medium with VEGF (R&D Systems) at the concentrations in Fig. 7D or 20 ng/mL VEGF with the inhibitor concentrations in Fig. 8B–D. Medium was added to the bottom chamber of CIM plates, and the bottom and top chambers were assembled prior to experimentation. iPSC-ECs between Passage 2–4 were seeded at 10000 cells $well^{-1}$ in a total volume of 100 μL in Starvation Medium with the inhibitor concentrations listed in Fig. 7 at 0.1 vol.% DMSO. Plates were incubated at 37°C, 5% $CO_2$, and 95% relative humidity for 24 hours with data collected every 15 minutes. After 24 hours, the final cell indices were correlated to the experimental conditions, which were performed in triplicate and compared via Student's t-test at p-value<0.05.

## Supplementary Material

Refer to Web version on PubMed Central for supplementary material.

## Acknowledgments

**Funding Sources**

The authors acknowledge support from the National Institutes of Health (NIH 1UH2 TR000506-01, 3UH2 TR000506-02S1, T32 HL007936-12, RO1 HL093282, and R21 EB016381-01).

## References Cited

1. Novosel EC, Kleinhans C, Kluger PJ. Vascularization is the key challenge in tissue engineering. Advanced Drug Delivery Reviews. 2011; 63(4–5):300–311. [PubMed: 21396416]
2. Phelps EA, García AJ. Engineering more than a cell: vascularization strategies in tissue engineering. Current Opinion in Biotechnology. 2010; 21(5):704–709. [PubMed: 20638268]
3. Nguyen EH, Zanotelli MR, Schwartz MP, Murphy WL. Differential effects of cell adhesion, modulus and VEGFR-2 inhibition on capillary network formation in synthetic hydrogel arrays. Biomaterials. 2014; 35(7):2149–2161. [PubMed: 24332391]
4. Moon JJ, Saik JE, Poche RA, Leslie-barbick JE, Smith AA, Dickinson ME, West JL. Biomimetic hydrogels with pro-angiogenic properties. Biomaterials. 2011; 31(14):3840–3847. [PubMed: 20185173]
5. Phelps EA, Landázuri N, Thulé PM, Taylor WR, García AJ. Bioartificial matrices for therapeutic vascularization. Proceedings of the National Academy of Sciences of the United States of America. 2010; 107(8):3323–3328. [PubMed: 20080569]
6. Chung S, Sudo R, Vickerman V, Zervantonakis IK, Kamm RD. Microfluidic Platforms for Studies of Angiogenesis, Cell Migration, and Cell–Cell Interactions. Annals of Biomedical Engineering. 2010; 38(3):1164–1177. [PubMed: 20336839]
7. Vickerman V, Blundo J, Chung S, Kamm R. Design, fabrication and implementation of a novel multi-parameter control microfluidic platform for three-dimensional cell culture and real-time imaging. Lab on a Chip. 2008; 8(9):1468–1477. [PubMed: 18818801]
8. Chrobak KM, Potter DR, Tien J. Formation of perfused, functional microvascular tubes in vitro. Microvascular research. 2006; 71(3):185–196. [PubMed: 16600313]
9. Moya ML, Hsu Y, Lee AP, Hughes CCW, George SC. In Vitro Perfused Human Capillary Networks. Tissue Engineering Part C. 2013; 19(9):730–737.
10. Kim S, Lee H, Chung M, Jeon NL. Engineering of functional, perfusable 3D microvascular networks on a chip. Lab on a chip. 2013; 13(8):1489–1500. [PubMed: 23440068]
11. Nolan DJ, Ginsberg M, Israely E, Palikuqi B, Poulos MG, James D, Rafii S. Molecular signatures of tissue-specific microvascular endothelial cell heterogeneity in organ maintenance and regeneration. Developmental cell. 2013; 26(2):204–219. [PubMed: 23871589]
12. Wetmore BA, Wambaugh JF, Ferguson SS, Li L, Clewell HJ, Judson RS, Thomas RS. Relative impact of incorporating pharmacokinetics on predicting in vivo hazard and mode of action from high-throughput in vitro toxicity assays. Toxicological Sciences. 2013; 132(2):327–346. [PubMed: 23358191]
13. Tice RR, Austin CP, Kavlock RJ, Bucher JR. Improving the human hazard characterization of chemicals: a Tox21 update. Environmental health perspectives. 2013; 121(7):756–765. [PubMed: 23603828]
14. Dix DJ, Houck KA, Judson RS, Kleinstreuer NC, Knudsen TB, Martin MT, Kavlock RJ. Incorporating biological, chemical, and toxicological knowledge into predictive models of toxicity. Toxicological Sciences. 2012; 130(2):440–441. [PubMed: 22982683]
15. Kleinstreuer NC, Judson RS, Reif DM, Sipes NS, Singh AV, Chandler KJ, Knudsen TB. Environmental impact on vascular development predicted by high-throughput screening. Environmental health perspectives. 2011; 119(11):1596–1603. [PubMed: 21788198]

16. Yu J, Vodyanik Ma, Smuga-Otto K, Antosiewicz-Bourget J, Frane JL, Tian S, Thomson Ja. Induced pluripotent stem cell lines derived from human somatic cells. Science. 2007; 318(5858): 1917–1920. [PubMed: 18029452]
17. Takahashi K, Tanabe K, Ohnuki M, Narita M, Ichisaka T, Tomoda K, Yamanaka S. Induction of pluripotent stem cells from adult human fibroblasts by defined factors. Cell. 2007; 131(5):861–872. [PubMed: 18035408]
18. Thomson JA, Itskovitz-Eldor J, Shapiro SS, Waknitz MA, Swiergiel JJ, Marshall VS, Jones JM. Embryonic Stem Cell Lines Derived from Human Blastocysts. Science. 1998; 282(5391):1145–1147. [PubMed: 9804556]
19. Hu K, Yu J, Suknuntha K, Tian S, Montgomery K, Choi K-D, Slukvin II. Efficient generation of transgene-free induced pluripotent stem cells from normal and neoplastic bone marrow and cord blood mononuclear cells. Blood. 2011; 117(14):e109–e119. [PubMed: 21296996]
20. Howden SE, Gore A, Li Z, Fung H-L, Nisler BS, Nie J, Thomson Ja. Genetic correction and analysis of induced pluripotent stem cells from a patient with gyrate atrophy. Proceedings of the National Academy of Sciences of the United States of America. 2011; 108(16):6537–6542. [PubMed: 21464322]
21. Ebert AD, Yu J, Rose FF, Mattis VB, Lorson CL, Thomson Ja, Svendsen CN. Induced pluripotent stem cells from a spinal muscular atrophy patient. Nature. 2009; 457(7227):277–280. [PubMed: 19098894]
22. Dimos JT, Rodolfa KT, Niakan KK, Weisenthal LM, Mitsumoto H, Chung W, Eggan K. Induced pluripotent stem cells generated from patients with ALS can be differentiated into motor neurons. Science (New York, N. Y.). 2008; 321(5893):1218–1221.
23. Kusuma S, Shen Y-I, Hanjaya-Putra D, Mali P, Cheng L, Gerecht S. Self-organized vascular networks from human pluripotent stem cells in a synthetic matrix. Proceedings of the National Academy of Sciences of the United States of America. 2013; 110(31):12601–12606. [PubMed: 23858432]
24. Kane NM, Xiao Q, Baker AH, Luo Z, Xu Q, Emanueli C. Pluripotent stem cell differentiation into vascular cells: a novel technology with promises for vascular re(generation). Pharmacology & therapeutics. 2011; 129(1):29–49. [PubMed: 20965210]
25. Choi K-D, Yu J, Smuga-Otto K, Salvagiotto G, Rehrauer W, Vodyanik M, Slukvin I. Hematopoietic and endothelial differentiation of human induced pluripotent stem cells. Stem Cells. 2009; 27(3):559–567. [PubMed: 19259936]
26. Wang L, Li L, Shojaei F, Levac K, Cerdan C, Menendez P, Bhatia M. Endothelial and hematopoietic cell fate of human embryonic stem cells originates from primitive endothelium with hemangioblastic properties. Immunity. 2004; 21(1):31–41. [PubMed: 15345218]
27. Levenberg S, Golub JS, Amit M, Itskovitz-Eldor J, Langer R. Endothelial cells derived from human embryonic stem cells. Proceedings of the National Academy of Sciences of the United States of America. 2002; 99(7):4391–4396. [PubMed: 11917100]
28. White MP, Rufaihah AJ, Liu L, Ghebremariam YT, Ivey KN, Cooke JP, Srivastava D. Limited gene expression variation in human embryonic stem cell and induced pluripotent stem cell-derived endothelial cells. Stem cells. 2013; 31(1):92–103. [PubMed: 23079999]
29. Voyta JC, Via DP, Butterfield CE, Zetter BR. Identification and isolation of endothelial cells based on their increased uptake of acetylated-low density lipoprotein. The Journal of cell biology. 1984; 99(6):2034–2040. Retrieved from http://www.pubmedcentral.nih.gov/articlerender.fcgi?artid=2113570&tool=pmcentrez&rendertype=abstract. [PubMed: 6501412]
30. Jackson CJ, Garbett PK, Nissen B, Schrieber L. Binding of human endothelium to Ulex europaeus I-coated Dynabeads: application to the isolation of microvascular endothelium. Journal of cell science. 1990; 96(Pt 2):257–262. Retrieved from http://www.ncbi.nlm.nih.gov/pubmed/2211866. [PubMed: 2211866]
31. Strawn LM, Mcmahon G, App H, Schreck R, Kuchler WR, Longhi MP, Shawver LK. Flk-1 as a Target for Tumor Growth Inhibition. Cancer Research. 1996; 56:3540–3545. [PubMed: 8758924]
32. Millauer B, Wizigmann-Voos S, Schnürch H, Martinez R, Møller NPH, Risau W, Ullrich A. High affinity VEGF binding and developmental expression suggest Flk-1 as a major regulator of

vasculogenesis and angiogenesis. Cell. 1993; 72(6):835–846. Retrieved from http://www.ncbi.nlm.nih.gov/pubmed/7681362. [PubMed: 7681362]

33. Ferrara N, Henzel WJ. Pituitary Follicular Cells Secrete a Novel Heparin-Binding Growth Factor Specific for Vascular Endothelial Cells. Biochemical and Biophysical Research Communications. 1989; 161(2):851–858. [PubMed: 2735925]
34. Mehta D, Malik AB. Signaling Mechanisms Regulating Endothelial Permeability. Physiology Reviews. 2006; 86:279–367.
35. Bardin N, Blot-Chabaud M, Despoix N, Kebir A, Harhouri K, Arsanto J-P, Dignat-George F. CD146 and its soluble form regulate monocyte transendothelial migration. Arteriosclerosis, thrombosis, and vascular biology. 2009; 29(5):746–753.
36. Gardner TW, Eller AW, Friberg TR, D'Antonio JA, Hollis TM. Antihistamines reduce blood-retinal barrier permeability in type I (insulin-dependent) diabetic patients with nonproliferative retinopathy. Retina. 1995; 15(2):134–140. [PubMed: 7624601]
37. Krause D, Mischeck U, Galla HJ, Dermietzel R. Correlation of zonula occludens ZO-1 antigen expression and transendothelial resistance in porcine and rat cultured cerebral endothelial cells. Neuroscience letters. 1991; 128(2):301–304. Retrieved from http://www.ncbi.nlm.nih.gov/pubmed/1945052. [PubMed: 1945052]
38. Moy AB, Blackwell K, Kamath A. Differential effects of histamine and thrombin on endothelial barrier function through actin-myosin tension. American journal of physiology. Heart and circulatory physiology. 2002; 282(1):H21–H29. Retrieved from http://www.ncbi.nlm.nih.gov/pubmed/11748043. [PubMed: 11748043]
39. Laposata M, Dovnarsky DK, Shin HS. Thrombin-induced gap formation in confluent endothelial cell monolayers. Blood. 1983; 62(3):549–556. [PubMed: 6309278]
40. Zervantonakis IK, Hughes-Alford SK, Charest JL, Condeelis JS, Gertler FB, Kamm RD. Three-dimensional microfluidic model for tumor cell intravasation and endothelial barrier function. Proceedings of the National Academy of Sciences of the United States of America. 2012; 109(34): 13515–13520. [PubMed: 22869695]
41. Folkman J, Haudenschild C. Angiogenesis in vitro. Nature. 1980; 288:551–556. [PubMed: 6160403]
42. Montesano R, Orci L, Vassalli P. In vitro rapid organization of endothelial cells into capillary-like networks is promoted by collagen matrices. The Journal of cell biology. 1983; 97(5 Pt 1):1648–1652. Retrieved from http://www.pubmedcentral.nih.gov/articlerender.fcgi?artid=2112683&tool=pmcentrez&rendertype=abstract. [PubMed: 6630296]
43. Grant DS, Tashiro K, Segui-Real B, Yamada Y, Martin GR, Kleinman HK. Two different laminin domains mediate the differentiation of human endothelial cells into capillary-like structures in vitro. Cell. 1989; 58(5):933–943. Retrieved from http://www.ncbi.nlm.nih.gov/pubmed/2528412. [PubMed: 2528412]
44. Kubota Y, Kleinman HK, Martin GR, Lawley TJ. Role of laminin and basement membrane in the morphological differentiation of human endothelial cells into capillary-like structures. The Journal of cell biology. 1988; 107(4):1589–1598. Retrieved from http://www.pubmedcentral.nih.gov/articlerender.fcgi?artid=2115245&tool=pmcentrez&rendertype=abstract. [PubMed: 3049626]
45. Leslie-Barbick JE, Saik JE, Gould DJ, Dickinson ME, West JL. The promotion of microvasculature formation in poly(ethylene glycol) diacrylate hydrogels by an immobilized VEGF-mimetic peptide. Biomaterials. 2011; 32(25):5782–5789. [PubMed: 21612821]
46. Leslie-Barbick JE, Moon JJ, West Jennifer L. Covalently-Immobilized Vascular Endothelial Growth Factor Promotes Endothelial Cell Tubulogenesis in Poly (ethylene glycol) Diacrylate Hydrogels. Journal of Biomaterials Science. 2009; 20:1763–1779.
47. Domansky K, Inman W, Serdy J, Dash A, Lim MHM, Griffith LG. Perfused multiwell plate for 3D liver tissue engineering. Lab on a chip. 2010; 10(1):51–58. [PubMed: 20024050]
48. Dewey CF, Bussolari SR, Gimbrone MA, Davies PF. The dynamic response of vascular endothelial cells to fluid shear stress. Journal of Biomechanical Engineering. 1981; 103(3):177–185. Retrieved from http://www.ncbi.nlm.nih.gov/pubmed/7278196. [PubMed: 7278196]
49. Ribatti D, Crivellato E. "Sprouting angiogenesis", a reappraisal. Developmental biology. 2012; 372(2):157–165. [PubMed: 23031691]

50. Haspel HC, Scicli GM, Mcmahon G, Scicli AG. Inhibition of Vascular Endothelial Growth Factor-Associated Tyrosine Kinase Activity with SU5416 Blocks Sprouting in the Microvascular Endothelial Cell Spheroid Model of Angiogenesis. Microvascular Research. 2002; 315:304–315. [PubMed: 11969307]
51. Potente M, Ghaeni L, Baldessari D, Mostoslavsky R, Rossig L, Dequiedt F, Dimmeler S. SIRT1 controls endothelial angiogenic functions during vascular growth. Genes & Development. 2007; 21(20):2644–2658. [PubMed: 17938244]
52. Germeroth L, Piossek C, Thierauch K-H, Schneider-Mergener J, Volkmer-Engert R, Bachmann MF, Augustin HG. Potent inhibition of angiogenesis by D,L-peptides derived from vascular endothelial growth factor receptor 2. Thrombosis and Haemostasis. 2003:501–510. [PubMed: 12958620]
53. Loges S, Roncal C, Carmeliet P. Development of targeted angiogenic medicine. Journal of Thrombosis and Haemostasis. 2009; 7(1):21–33. [PubMed: 18983480]
54. Mabeta P, Pepper MS. A comparative study on the anti-angiogenic effects of DNA-damaging and cytoskeletal-disrupting agents. Angiogenesis. 2009; 12:81–90. [PubMed: 19214765]
55. Nakatsu MN, Sainson RCA, Aoto JN, Taylor KL, Aitkenhead M, Pérez-del-Pulgar S, Hughes CCW. Angiogenic sprouting and capillary lumen formation modeled by human umbilical vein endothelial cells (HUVEC) in fibrin gels: the role of fibroblasts and Angiopoietin-1☆. Microvascular Research. 2003; 66(2):102–112. [PubMed: 12935768]
56. Barkefors I, Le Jan S, Jakobsson L, Hejll E, Carlson G, Johansson H, Kreuger J. Endothelial cell migration in stable gradients of vascular endothelial growth factor A and fibroblast growth factor 2: effects on chemotaxis and chemokinesis. Journal of Biological Chemistry. 2008; 283(20): 13905–13912. [PubMed: 18347025]
57. Van Horssen R, Galjart N, Rens JaP, Eggermont AMM, ten Hagen TLM. Differential effects of matrix and growth factors on endothelial and fibroblast motility: application of a modified cell migration assay. Journal of cellular biochemistry. 2006; 99(6):1536–1552. [PubMed: 16817234]
58. Staton CA, Reed MWR, Brown NJ. A critical analysis of current in vitro and in vivo angiogenesis assays. International journal of experimental pathology. 2009; 90(3):195–221. [PubMed: 19563606]
59. Chi J-T, Chang HY, Haraldsen G, Jahnsen FL, Troyanskaya OG, Chang DS, Brown PO. Endothelial cell diversity revealed by global expression profiling. Proceedings of the National Academy of Sciences of the United States of America. 2003; 100(19):10623–10628. [PubMed: 12963823]
60. Rufaihah AJ, Huang NF, Kim J, Herold J, Volz KS, Park TS, Cooke JP. Human induced pluripotent stem cell-derived endothelial cells exhibit functional heterogeneity. American Journal of Translational Research. 2013; 5(1):21–35. Retrieved from http://www.pubmedcentral.nih.gov/articlerender.fcgi?artid=3560482&tool=pmcentrez&rendertype=abstract. [PubMed: 23390563]
61. Carmeliet P. Mechanisms of angiogenesis and arteriogenesis. Nature Medicine. 2000; 6(4):389–395.
62. Woad KJ, Hunter MG, Mann GE, Laird M, Hammond AJ, Robinson RS. Fibroblast growth factor 2 is a key determinant of vascular sprouting during bovine luteal angiogenesis. Reproduction. 2012; 143(1):35–43. [PubMed: 21998077]
63. Mavria G, Vercoulen Y, Yeo M, Paterson H, Karasarides M, Marais R, Marshall CJ. ERK-MAPK signaling opposes Rho-kinase to promote endothelial cell survival and sprouting during angiogenesis. Cancer Cell. 2006; 9(1):33–44. [PubMed: 16413470]
64. Oikawa T, Shimamura M, Ashino H. Inhibition of Angiogenesis by Staurosporine, a Potent Protein Kinase Inhibitor. Journal of Antibiotics. 1992; 45(7):1155–1160. [PubMed: 1381345]
65. Liu T-C, Branco CP, Rabkin SD, Martuza RL. Trichostatin A and Oncolytic HSV Combination Therapy Shows Enhanced Antitumoral and Antiangiogenic Effects. Molecular Therapy. 2008; 16(6):1041–1047. [PubMed: 18388912]
66. O'Farrell A-M, Abrams TJ, Yuen HA, Ngai TJ, Louie SG, Yee KWH, Cherrington JM. SU11248 is a novel FLT3 tyrosine kinase inhibitor with potent activity in vitro and in vivo. Blood. 2003; 101(9):3597–3605. [PubMed: 12531805]

67. Spiekermann K, Faber F, Voswinckel R, Hiddemann W. The protein tyrosine kinase inhibitor SU5614 inhibits VEGF-induced endothelial cell sprouting and induces growth arrest and apoptosis by inhibition of c-kit in AML cells. Experimental Hematology. 2002; 30(7):767–773. Retrieved from http://www.ncbi.nlm.nih.gov/pubmed/12135675. [PubMed: 12135675]

68. Sun L, Tran N, Liang C, Hubbard S, Tang F, Lipson K, Schreck R. Identification of Substituted 3-[(4,5,6,7-Tetrahydro-1H-indol-2-yl)methylene]- 1,3-dihydroindol-2-ones as Growth Factor Receptor Inhibitors for VEGF-R2 (Flk-1 / KDR), FGF-R1, and PDGF-R Tyrosine Kinases. Journal of Medicinal Chemistry. 2000; 43:2655–2663. [PubMed: 10893303]

69. Korff T, Augustin HG. Tensional forces in fibrillar extracellular matrices control directional capillary sprouting. Journal of Cell Science. 1999; 112:3249–3258. Retrieved from http://www.ncbi.nlm.nih.gov/pubmed/10504330. [PubMed: 10504330]

70. Murakami M, Nguyen LT, Zhang ZW, Moodie KL, Carmeliet P, Stan RV, Simons M. The FGF system has a key role in regulating vascular integrity. Journal of Clinical Investigation. 2008; 118(10):3355–3366. [PubMed: 18776942]

71. Ellis LM, Hicklin DJ. VEGF-targeted therapy: mechanisms of anti-tumour activity. Nature Reviews. Cancer. 2008; 8(8):579–591.

72. Woad KJ, Hammond AJ, Hunter M, Mann GE, Hunter MG, Robinson RS. FGF2 is crucial for the development of bovine luteal endothelial networks in vitro. Reproduction (Cambridge, England). 2009; 138(3):581–588.

73. Yoshida A, Anand-apte B, Zetter BR. Differential Endothelial Migration and Proliferation to Basic Fibroblast Growth Factor and Vascular Endothelial Growth Factor. Growth Factors. 1996; 13(1–2):57–64. [PubMed: 8962720]

74. Herbert SP, Stainier DYR. Molecular control of endothelial cell behaviour during blood vessel morphogenesis. Nature Reviews. Molecular Cell biology. 2011; 12(9):551–564.

75. Whisler JA, Chen MB, Kamm RD. Control of Perfusable Microvascular Network Morphology Using a Multiculture Microfluidic System. 2013; 00(00)

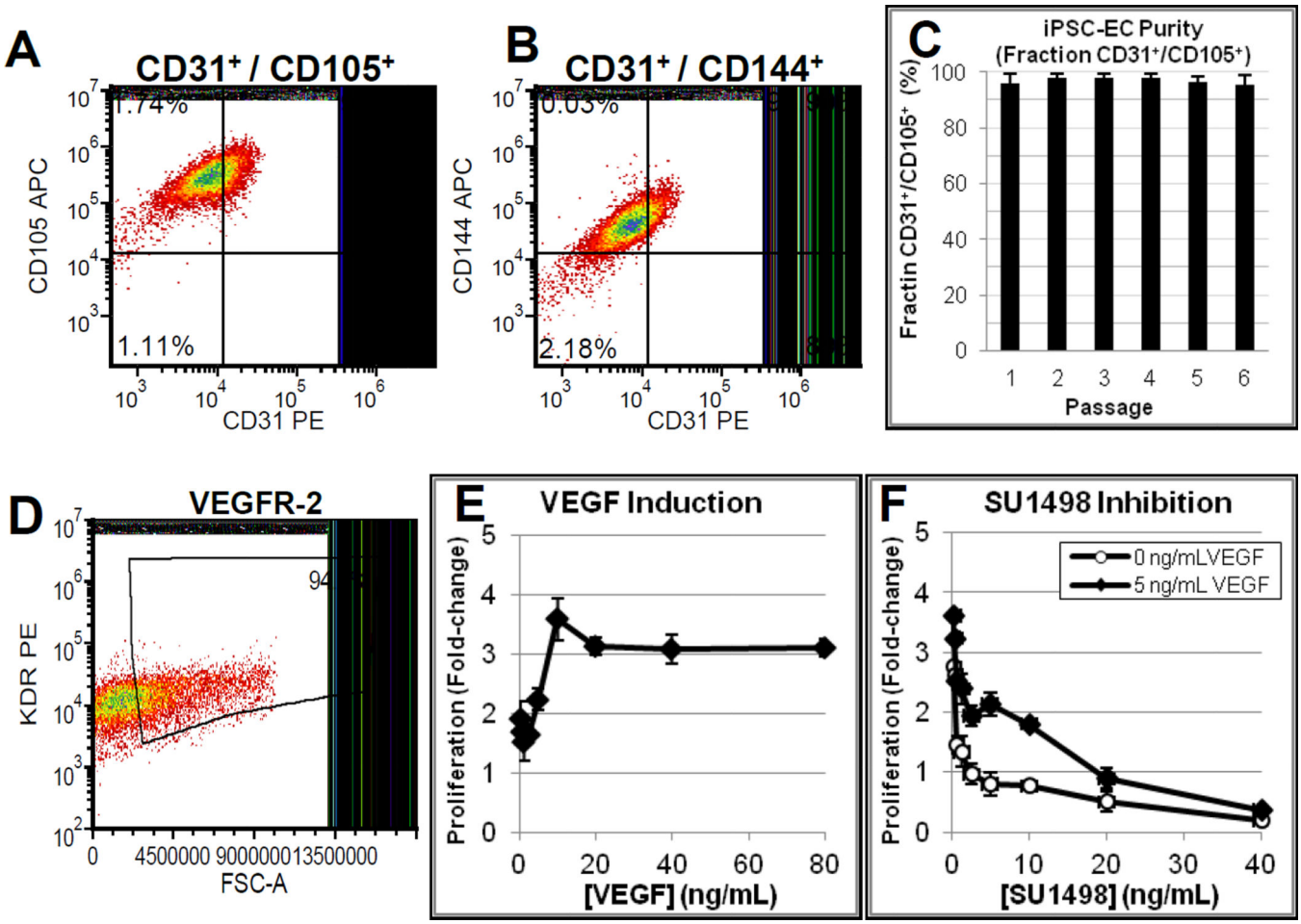


**Figure 1. iPSC-ECs stably express common endothelial cell markers and proliferate in response to VEGF/VEGFR2 signaling**

**(A)** FACs analysis for PECAM / Endoglin co-expression.

**(B)** FACs analysis illustrating PECAM / VE-cadherin co-expression.

**(C)** iPSC-ECs maintain purity for at least 6 passages based on FACs analysis of CD31/ CD105 co-expression. Average of 3 separate lots, 3 thaws each (9 samples total). Error bars = S.D.

**(D)** FAC analysis for iPSC-EC expression of VEGFR-2 (KDR/Flk1). iPSC proliferation in response to **(E)** VEGF treatment (in Starvation Medium), and **(F)** when treated with the VEGFR-2 inhibitor SU1498 in Starvation Medium with 0 (white diamonds) or 5 ng/mL VEGF (black diamonds).

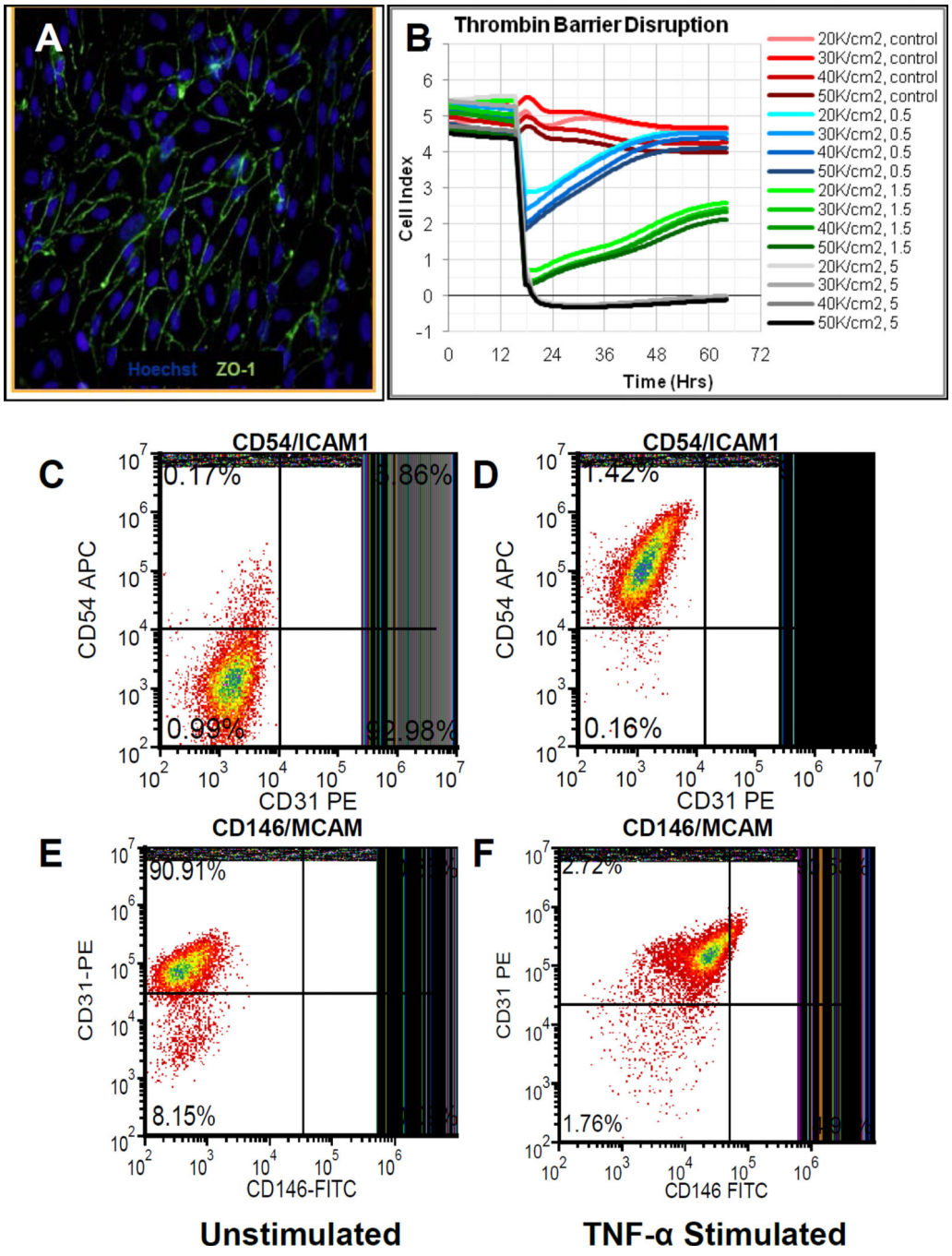


**Figure 2. iPSC-EC expression and function**

**(A)** iPSC-ECs express ZO-1 tight junction protein at cell borders.

**(B)** iPSCs exhibit thrombin-dependent barrier function. Traces in red represent control conditions without thrombin. Blue, green, and black traces represent cell index over time in the presence of thrombin at 0.5 U/mL, 1.5 U/mL, or 5 U/mL respectively.

**(C–F)** Upregulation of cell adhesion molecules **(C–D)** CD54 (ICAM1) and **(E–F)** CD146 (MCAM) for iPSC-ECs in response to treatment with 25 μg/mL TNF-α for 24 hours.

ICAM1 expression **(C)** before and **(D)** after TNF-α treatment. MCAM expression **(E)** before and **(F)** after TNF-α treatment.

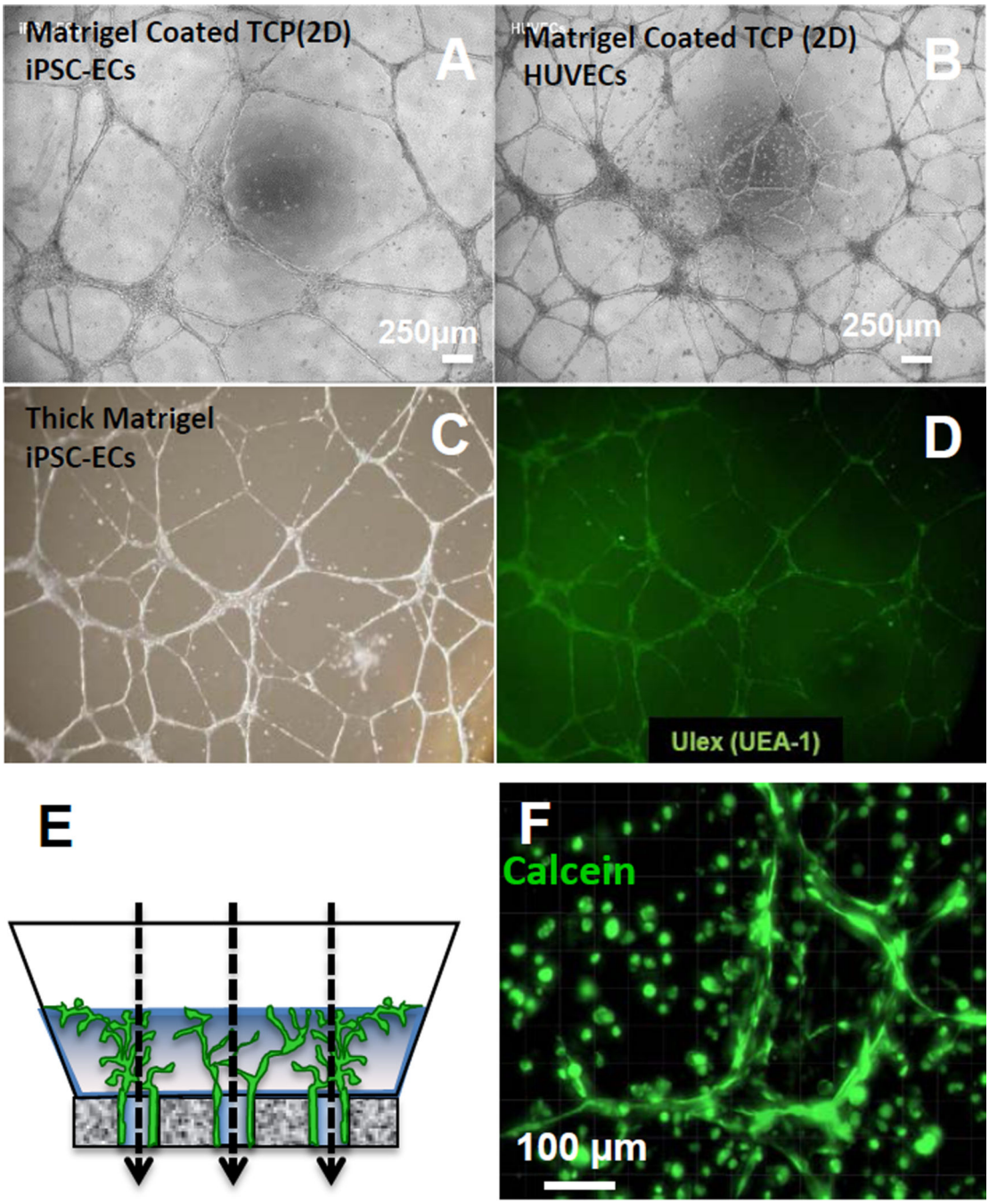


**Figure 3. Tube forming assays for endothelial cells in 2D and 3D environments**

**(A–B)** 2D tube-forming assay on Matrigel (coated TCP plate) for **(A)** iPSC-ECs and **(B)** HUVECs.

**(C–D)** 3D tube-forming assay for iPSC-ECs in a thick layer of Matrigel; **(C)** Brightfield microscopy and **(D)** UEA-1 fluorescence imaging. UEA-1 is highly specific for EC lectin (fucose) [**Jackson, JCS 1990**].

**(E)** Schematic of 3D iPSC-EC encapsulation in Matrigel within a custom bioreactor to provide flow in the direction of the dashed arrows.

**(F)** Maximum intensity projection of iPSC-ECs encapsulated in Matrigel (3D) and stained with Calcein-AM after 2 days of culture in the bioreactor from **(E)**.

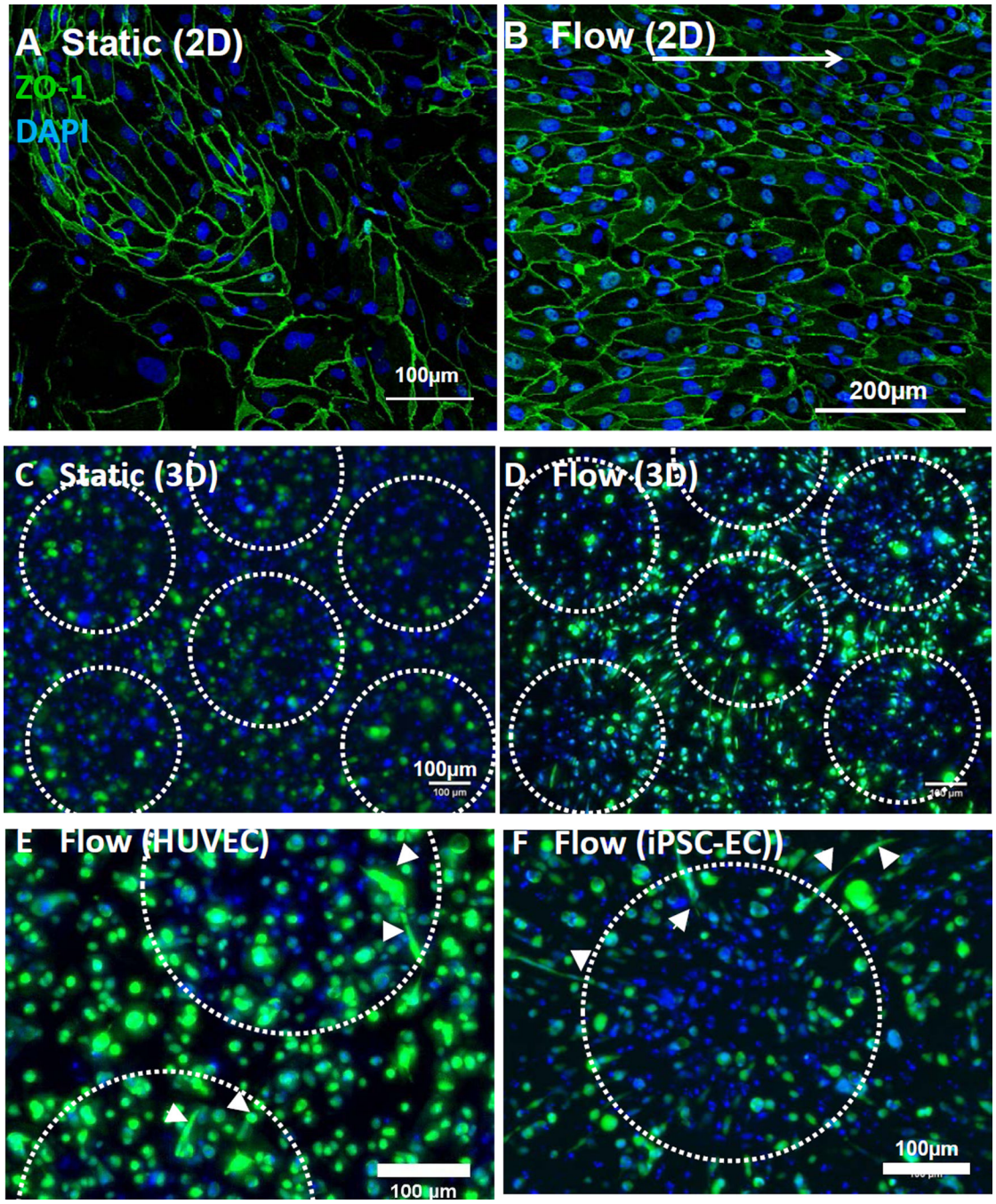


**Figure 4. iPSC-EC organization when subjected to flow**

**(A–B)** iPSC-ECs cultured in a microfluidics channel and subjected to lateral flow (shear stress = 20 dyn/cm$^2$) to verify the capacity for alignment. Cells were randomly oriented without flow **(A)** but adopted elongated morphologies in the direction of an applied (left to right) shear stress **(B)**.

**(C–D)** Representative maximum intensity projection of iPSC-ECs encapsulated in Matrigel and cultured in a bioreactor for 4 days (as shown in Fig. 3E). Cells exhibited a rounded morphology in the absence of flow, but adopted an extended morphology towards the

central axis of flow along the periphery of each channel. Channels were formed from 340μm pores (outlined in dotted white line) wherein flow was provided in the z-direction (into the frame of the micrographs. Z-stack = 300μm, z-slice thickness = 3μm
**(E–F)** Representative maximum intensity projections of HUVECs **(E)** and iPSC-ECs **(F)** cultured in bioreactor (schematic Fig. 3E). Cells in the presence of flow exhibited an elongated morphology towards the central axis of flow (denoted by white arrowheads). Z-stack = 300μm, z-slice thickness = 3μm

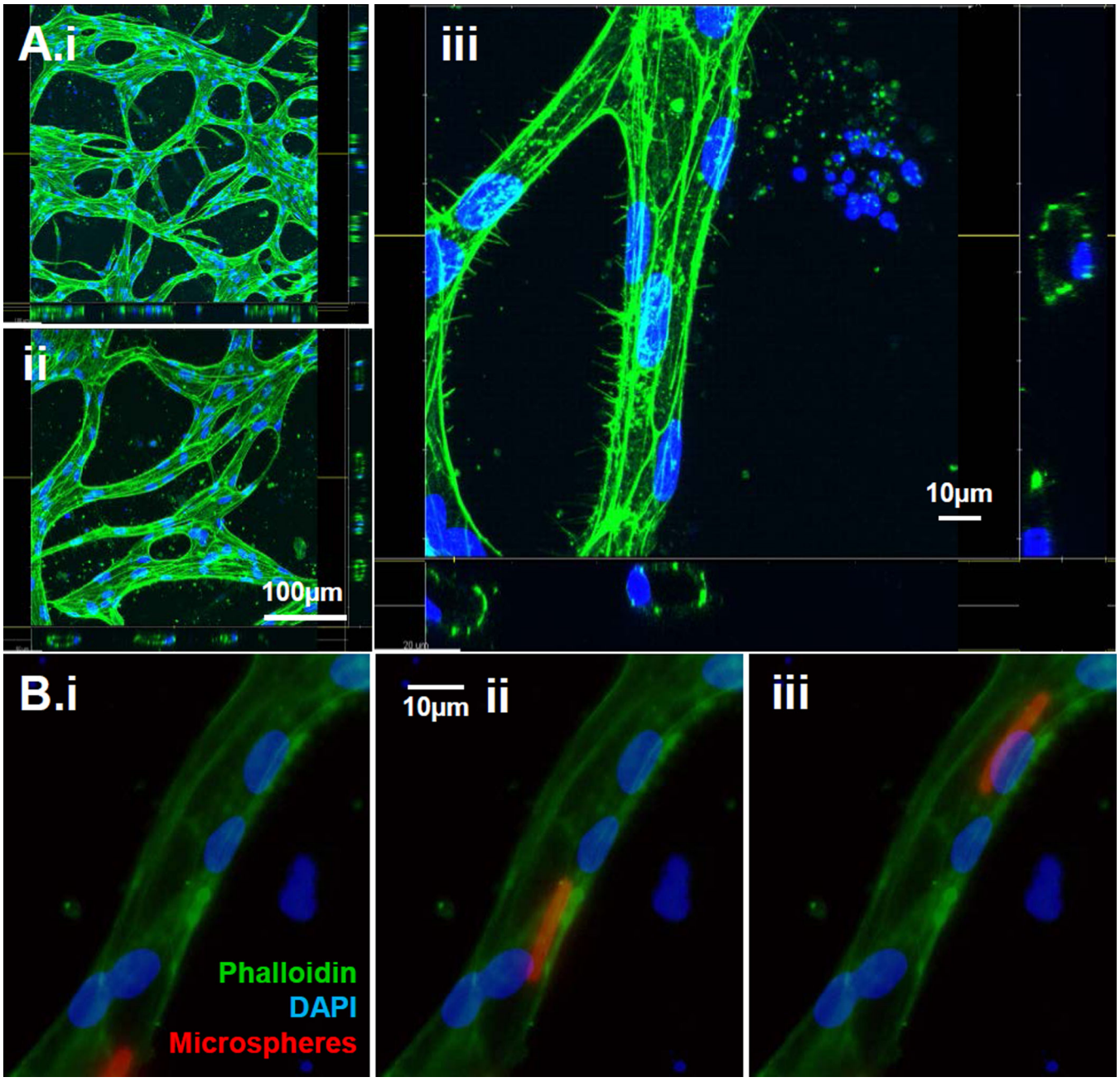


**Figure 5. iPSC-ECs form perfusable capillaries in a microfluidics device**

iPSC-ECs encapsulated in fibrin within a central microfluidics channel with adjacent channels containing encapsulated fibroblasts.

**(A)** After 4 days in culture with S1P-containing medium, iPSC-ECs encapsulated in central chamber were stained with FITC-Phalloidin and DAPI and were imaged using confocal laser scanning microscopy **(A.i–ii)**. Scale bar: 100 µm **(A.iii)** Confocal image of iPSC-ECs stained with FITC-Phalloidin and DAPI, demonstrating that tubules contained a hollow lumen. Scale bar: 10µm

**(B)** 4µm fluorescent microspheres were added to the channel and constrained to endothelial cell-lined tubes, demonstrating that iPSC-EC tubules were perfusable over time (Time scale

= 119ms). Microspheres appear as a streak of ~15μm indicating movement in a given shutter exposure. Scale bar: 10 μm

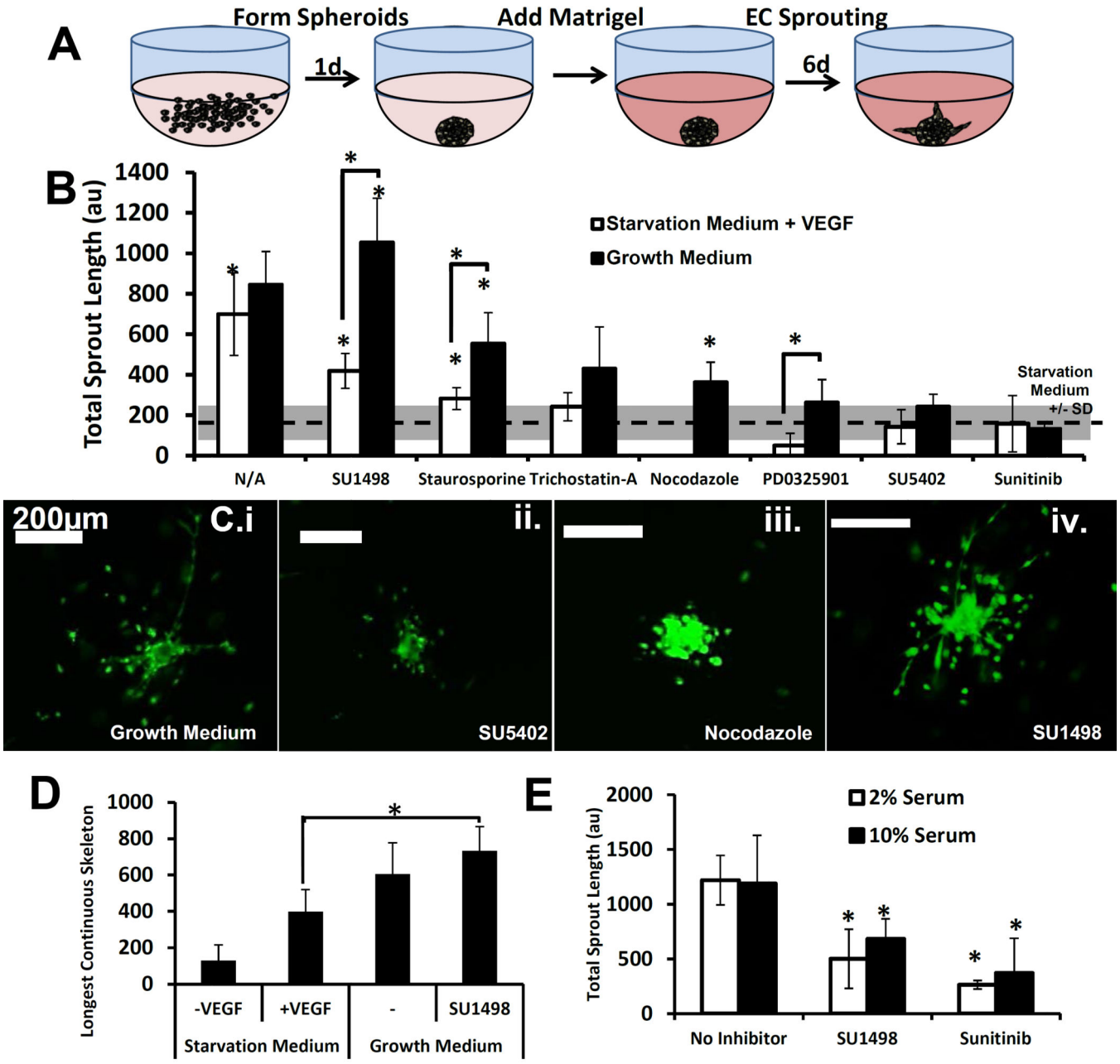


**Figure 6. VEGF/VEGFR2 signaling is necessary but not sufficient to induce iPSC-EC sprouting**

**(A)** Schematic of cell spheroid formation in round-bottom low adhesion plates using Matrigel as a substrate to enable iPSC-EC sprouting. Analysis was performed after 7 total days in culture using Calcein-AM.

**(B)** Quantification of total sprout length of iPSC-ECs cultured in a VEGF-only solution or Full Supplement (containing VEGF, FGF-2, IGF-1, and EGF) along with a library of pharmacological inhibitors. The control condition with 10 vol.% serum and no growth factors is shown by a dashed line, and +/1 standard deviation is shown as a gray bar. Statistical significance compared to the control is denoted for p-value < 0.05 (*).

**(C)** Fluorescent micrographs demonstrating sprouting after 6 full days in culture with Matrigel. Cells were stained with Calcein-AM and Ethidium Homodimer-1. Scale bar represents 200 μm. Image series demonstrates sprouting in the presence of growth medium (C.i) with SU5402 (ii), nocodazole (iii.), or SU1498 (iv.).

**(D)** Quantification of mean length of longest branched sprout in a subset of conditions in **(B)**, showing increased longest continuous skeleton in SU1498-containing medium with Growth Medium. Statistical significance compared to the conditions in brackets is denoted for p-value < 0.05 (*).

**(E)** Total sprout length as a function of VEGF in 2 and 10 vol.% serum with no inhibitor, SU1498, or Sunitinib. Statistical significance compared to no inhibitor conditions denoted for p-value < 0.05 (*)

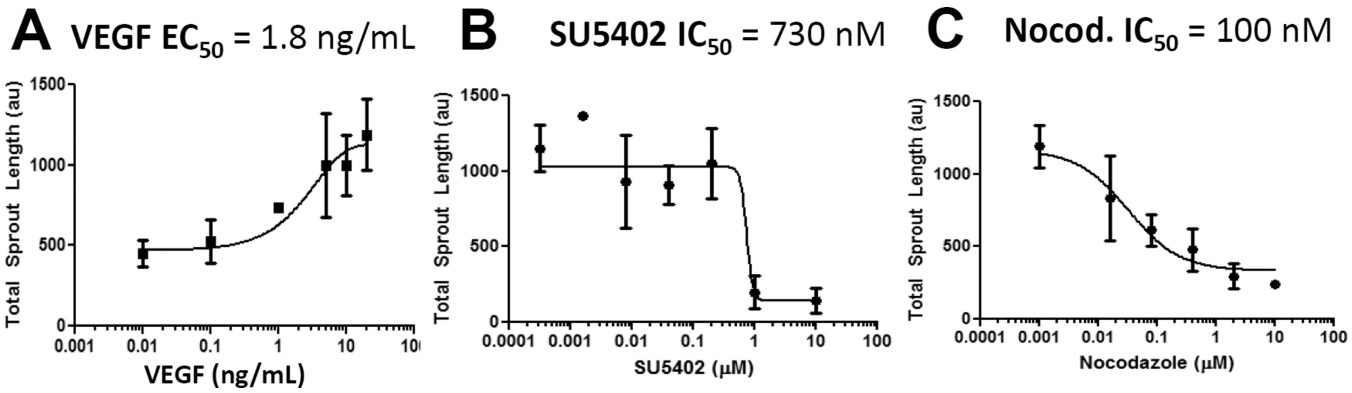


**Figure 7. iPSC-EC sprouting depends on both VEGF signaling and microtubule polymerization**

**(A)** iPSC-EC total sprout length as a function of VEGF concentration. Sigmoidal regression analysis was used to calculate an $EC_{50}$ value for VEGF.

**(B,C)** Analysis of sprouting inhibition with SU5402 **(B)** and nocodazole **(C)** at a range of concentrations. Sigmoidal regression analysis was used to calculate an $IC_{50}$ value for each inhibitor.

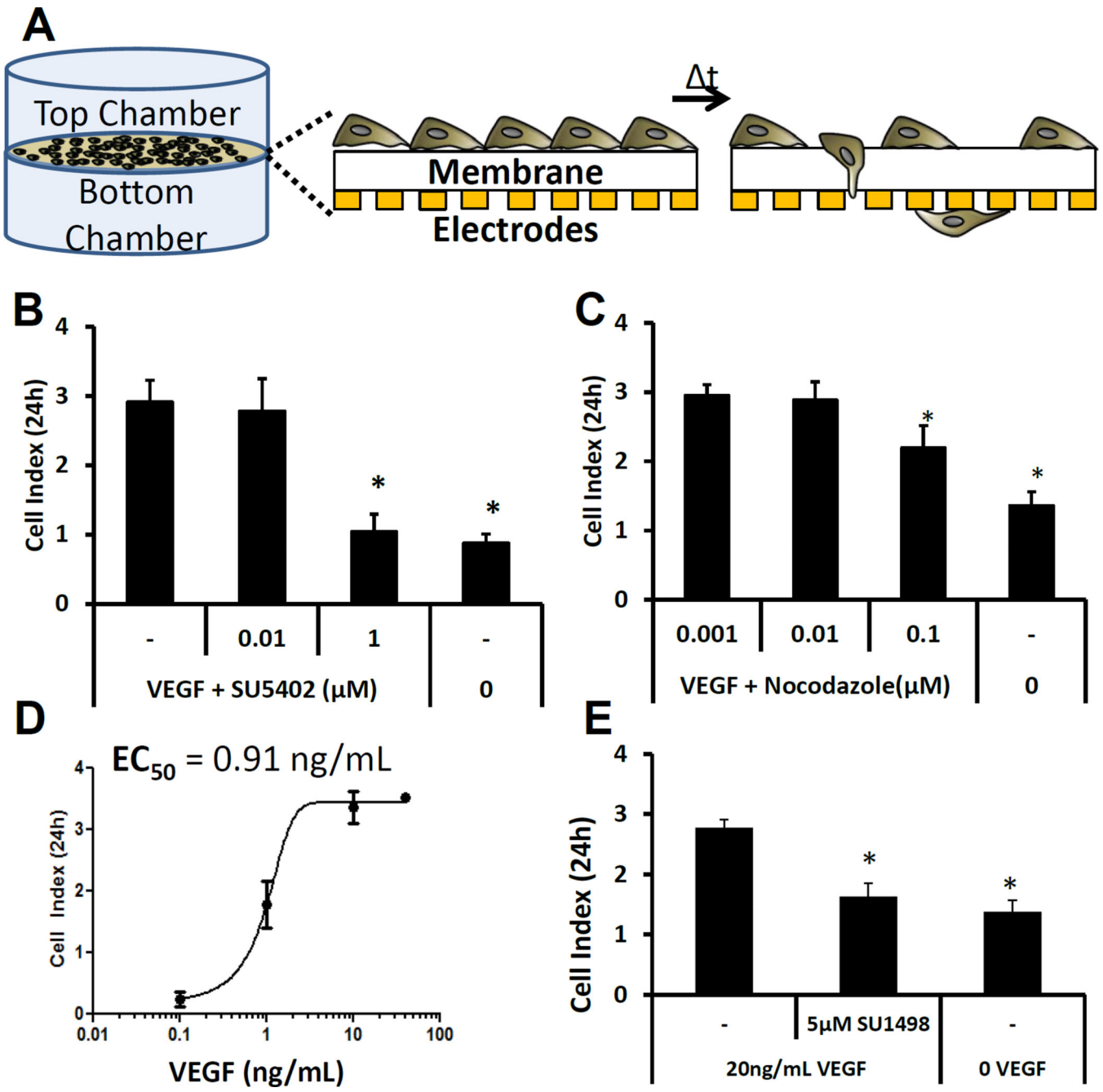


**Figure 8. iPSC-EC migration is dependent on VEGF/VEGFR2 signaling and microtubule organization**

**(A,B)** End-point analysis of iPSC-EC migration quantified using real-time impedance measurements in different concentrations of SU5402 **(A)** or nocodazole **(B)** in medium containing 10 vol.% serum with 20ng/mL VEGF in the bottom chamber and 10 vol.% serum and no VEGF in the top chamber. Statistical significance compared to the control without inhibitor is denoted is denoted for p-value < 0.05 (*).

**(C)** End-point analysis of iPSC-EC migration in different concentrations of VEGF, added only to the bottom chamber. Sigmoidal regression analysis was used to calculate an $EC_{50}$ value for VEGF

**(D)** End-point analysis of iPSC-EC migration in the presence of the VEGF receptor tyrosine kinase inhibitor SU1498. Statistical significance compared to the no inhibitor control is denoted for p-value < 0.05 (*).